



Article

# Comparative Spectroscopic and Electrochemical Study of V(V)-Substituted Keggin-Type Phosphomolybdates and -Tungstates

Jan-Christian Raabe , José Aceituno Cruz , Jakob Albert and Maximilian J. Poller \*

Institute for Technical and Macromolecular Chemistry, Universität Hamburg, Bundesstraße 45, 20146 Hamburg, Germany

\* Correspondence: maximilian.poller@uni-hamburg.de

**Abstract:** Vanadium-substituted Keggin-type heteropolyanions have been studied for a wide variety of applications, ranging from catalysis to antiviral/antimicrobial agents. While the V-substituted phosphomolybdates  $[PV_xMo_{12-x}O_40]^{(3+x)-}$  have been well investigated in this context, comparatively little is known about the corresponding phosphotungstates  $[PV_xW_{12-x}O_40]^{(3+x)-}$ . We have succeeded in synthesizing the sodium salts of the whole series  $[PV_xW_{12-x}O_40]^{(3+x)-}$ , for  $x = 1$  to 6, and characterised them spectroscopically (FT-IR, UV-Vis,  $^{31}P$ - and  $^{51}V$ -NMR) and electrochemically (CV and SWV). Thereby, direct comparisons between the vanadium-substituted phosphomolybdates and -tungstates, with substitution degrees from 1 to 6, can be established, which provides a solid basis for further investigations of potential applications.

**Keywords:** polyoxometalates; heteropolyanions; spectroscopy; electrochemistry; phosphotungstates; phosphomolybdates; vanadium



**Citation:** Raabe, J.-C.; Aceituno Cruz, J.; Albert, J.; Poller, M.J. Comparative Spectroscopic and Electrochemical Study of V(V)-Substituted Keggin-Type Phosphomolybdates and -Tungstates. *Inorganics* **2023**, *11*, 138. <https://doi.org/10.3390/inorganics11040138>

Academic Editor: Greta Ricardo Patzke

Received: 24 February 2023

Revised: 9 March 2023

Accepted: 17 March 2023

Published: 23 March 2023



**Copyright:** © 2023 by the authors. Licensee MDPI, Basel, Switzerland. This article is an open access article distributed under the terms and conditions of the Creative Commons Attribution (CC BY) license (<https://creativecommons.org/licenses/by/4.0/>).

## 1. Introduction

Polyoxometalates (POMs), especially those substituted with redox-active transition metals such as Vanadium (V), are used for a wide variety of applications, ranging from catalysis to the biomedical field. Examples of catalytic applications are, the conversion of biomass to formic acid and the oxidative catalytic desulfurization of fuels [1–9]. In the field of biomedicine, vanadium-containing POMs have shown antibacterial and antiviral effects, as well as anti-tumour properties [10–14].

The antibacterial activity of POMs was discovered in 1993, by Tajima et al. [15], and can be attributed to synergistic and direct antibacterial activity. Numerous POMs show no antibacterial activity on their own but become active in synergy with conventional antibiotics. The discovery of this property, first led to the discovery of the antibacterial phosphotungstate species known as “Factor T”, which was later identified as the lacunary anion  $[PW_{11}O_{39}]^{7-}$  [11,15]. However, this effect was only shown in synergy with  $\beta$ -lactam antibiotics, against the bacterial strains *Staphylococcus epidermidis* and *Staphylococcus auricularis* [13]. Based on these discoveries, various POM structures, especially tungstate structures, were identified as active [11]. A few POMs exhibit antibacterial properties, even without the addition of another antibiotic, including some tungsten and vanadium clusters. In addition, antibacterial properties of Keggin-type POMs  $H_3[PMo_{12}O_40]$  HPMo,  $H_3[PW_{12}O_40]$  HPW, and  $H_4[SiW_{12}O_40]$  HSiW, against the bacteria *Escherichia coli* (Gram-negative) and *Bacillus subtilis* (Gram-positive), are also known. The effect is triggered photocatalytically, by irradiation with UV light [11]. Antiviral activity of some V(V)-substituted tungstate structures was also confirmed in various in vitro and in vivo assays, against RNA viruses [12]. Thus, in vitro antiviral activities against HI virus were found, with the POM presumably binding to the gp-120 protein and thus interfering with the interaction of the anti-gp-120 antibody with the gp-120 protein [16]. In further studies, it was shown

that, especially tungstate-based POMs, also have the ability to inhibit DNA polymerase in retroviruses and thus show antiviral activity against the HIV virus [14]. Another biomedical application of POMs is the anti-tumour effect of molybdenum-based POMs, induced by cell apoptosis. Presumably, the POM is preferentially taken up by tumour cells, where it is metabolised to a more toxic compound, that inhibits ATP generation. However, the mechanisms of the anti-tumour action of POMs are still the subject of current research [14].

Furthermore, the current interest in POMs is illustrated by a number of novel applications to current research topics. For example, the research group of Schimpf, demonstrated that POM anions can be used to create tuneable functional materials, by connecting POM anions with suitable transition metal cations [17,18].

This shows that, especially the tungsten-based POMs are of great interest for biomedical research. However, in contrast to the vanadium-substituted phosphomolybdates ( $[PV_xMo_{12-x}O_{40}]^{(3+x)-}$ ,  $x = 1$  to 6), which have been comprehensively investigated in the context of catalysis, the corresponding tungstates ( $[PV_xW_{12-x}O_{40}]^{(3+x)-}$ ) have not been studied as thoroughly.

The synthesis of tailor-made, transition metal-substituted POMs, can be generally achieved by two different strategies. In a self-assembly synthesis, the precursor compounds are combined in a defined stoichiometry, and under suitable reaction conditions, the monomeric precursor species then link, to form oligomeric cluster structures. Such synthesis strategies have been shown to be robust against pH fluctuations. Furthermore, high degrees of substitution with foreign metals, i.e., V(V), can be achieved. The synthesis of V-substituted phosphomolybdates, reported by Odyakov et al., is based on this strategy [19–22]. The second possibility is the lacunary approach. Here, the synthesis route starts from an intact (usually commercially available) POM structure. Under basic conditions, individual metal–oxygen polyhedra are dissolved out of the POM network, forming a defect POM structure containing vacancies (usually one to three vacancies), known as a lacunary POM structure [23]. The vacancies can now be filled with other metals, resulting in transition metal-substituted POM structures. This method is commonly utilised for the synthesis of substituted Keggin-tungstates. However, POM lacunary structures can be susceptible to pH fluctuations, as they are often stable only within a small pH window. Low degrees of substitution also result, since the theoretically maximum possible number of vacancies is severely limited [23–25].

We have adapted the self-assembly strategy, to successfully synthesise the  $[PV_xW_{12-x}O_{40}]^{(3+x)-}$  for  $x$  up to 6. In this work, we present the resulting new heteropoly-anions, with their spectroscopic and electrochemical characteristics, in comparison with the corresponding molybdates.

## 2. Results and Discussion

The POMs  $H_{3+x}[PV_xMo_{12-x}O_{40}]$  ( $HPV_xMo$ ), with  $x = 1$  to 6, were synthesised according to the adapted literature procedure of Odyakov et al. [20–22], using molybdenum trioxide  $MoO_3$ , phosphoric acid  $H_3PO_4$ , and divanadium pentoxide  $V_2O_5$ .  $Na_{3+x}[PV_xW_{12-x}O_{40}]$  ( $NaPV_xW$ ), with  $x = 2$  to 3, were synthesised from the previously synthesised lacunary POM  $[PW_9O_{34}]^{9-}$  species, whereas the POMs  $NaPV_xW$ , with  $x = 4$  to 6, were synthesised starting from  $Na_2WO_4$ ,  $NaVO_3$ , and  $H_3PO_4$ , using a self-assembly approach. Compound  $NaPVW$  was synthesised via *in situ* lacunary  $[PW_{11}O_{39}]^{7-}$  formation, starting from commercially available phosphotungstic acid hydrate (HPW) [26–30]. Since sodium-containing precursors were used for the synthesis of  $NaPV_xW$ , the POMs could only be isolated as sodium salts. The fact that the  $HPV_xMo$  analogues can be obtained as free acids in solution is due to the different synthetic strategy used, since for the molybdates, an alkali ion free synthesis from the respective metal oxides is possible. However, this approach is not suitable for the tungstate analogues, since the  $WO_3$  does not present solubility properties compatible with the Keggin-type POM synthesis. Nevertheless, it is desirable to isolate the corresponding heteropolyacids. For example, in a study by Albert et al., (2014) [5], it was shown that catalytic applications of POMs in biomass conversion require bifunctional compounds, that

ensure the conversion of the substrate by acid/base catalysis (hydrolysis of the substrate), followed by redox catalysis (substrate oxidation). Thus, it could be advantageous to combine the acid/base effect, with the anion-mediated redox properties, in one molecule. In order to obtain bifunctional POMs, combining the acid/base and redox components, a suitable strategy was sought, to ensure the conversion of the obtained POM salts to their free acids. It was described by Tsigdinos et al. [31], that the free POM acids can be generated from the corresponding alkali salts by extraction of the POM with diethyl ether. However, this method failed in the attempt to obtain higher degrees of substitution than  $x = 3$  [31]. In our experimental results (for details see Supporting Information), it was found that the yields of the extracted free acid decreases with increasing degree of substitution (61% for the formation of HPW from NaPVW, 23% for HPV<sub>2</sub>W from NaPV<sub>2</sub>W, and only 3% for HPV<sub>3</sub>W from NaPV<sub>3</sub>W). In the case of NaPV<sub>4</sub>W, the method failed completely. This result is consistent with the data found for the molybdates described by Tsigdinos et al. [31]. In addition, significant losses of the metals W(VI) and V(V) from the Keggin-structure, are observed already from a substitution level of 2, which leads to an additional limitation of this method for practical use (see Table 1).

Table 1 summarises the results obtained from the elemental analysis (AAS/ICP-OES), and from the TGA analysis. For interpretation, all results were normalised to the framework metal molybdenum or tungsten, respectively. The phosphorous content in the V(V)-substituted phosphomolybdates is increased, due to the excess of phosphoric acid used during the synthesis, as suggested by Odyakov et al. [20–22]. The elemental analysis method used to determine the tungsten content, has a systematic error, which causes the tungsten content to be determined too low, with the result that the contents of the other elements appear to be too high in relation to it, since the corresponding framework metals (tungsten in this case) were normalised for interpretation. When considering the POMs NaPVW to NaPV<sub>3</sub>W, it can be assumed that the charge balance of the anions is completely ensured by the sodium cations, while for the POMs NaPV<sub>4</sub>W to NaPV<sub>6</sub>W, a lower cation content was found than would be necessary for a complete charge balance. The remaining charge balance can therefore only be ensured by protons originating from the acidic medium during synthesis. Thus, compounds NaPV<sub>4</sub>W to NaPV<sub>6</sub>W were obtained as mixed salts/ acids. One possible reason for this, is that the tungstates with  $x = 1$  to 3 and  $x = 4$  to 6, were prepared by two different synthetic approaches (lacunary vs. self-assembly approach). However, it is also conceivable that the increased charge of the POM anions increases their basicity, which increases with increasing degree of substitution. This can lead to the heteropolyacid not dissociating completely in aqueous media, which means that not all protons can be exchanged by sodium ions.

**Table 1.** Results from AAS/ICP-OES and TGA analyses of the different POMs analysed in this work.

Compound	Molecular Composition	Element Ratio	Hydration Water [mol/mol-POM]
HPVMo	H <sub>4</sub> [PVMo <sub>11</sub> O <sub>40</sub> ]	P/V/Mo 1.23 <sup>a</sup> /0.97/11	7
HPVW	H <sub>4</sub> [PVW <sub>11</sub> O <sub>40</sub> ]	Na/P/V/W 0/1.08/1.07/11 <sup>b</sup>	18
NaPVW	Na <sub>4</sub> [PVW <sub>11</sub> O <sub>40</sub> ]	Na/P/V/W 4.05/1.15 <sup>b</sup> /1.18 <sup>b</sup> /11 <sup>b</sup>	9
HPV <sub>2</sub> Mo	H <sub>5</sub> [PV <sub>2</sub> Mo <sub>10</sub> O <sub>40</sub> ]	P/V/Mo 1.28 <sup>a</sup> /2.01/10	9
HPV <sub>2</sub> W	H <sub>5</sub> [PV <sub>2</sub> W <sub>10</sub> O <sub>40</sub> ]	Na/P/V/W 0/1.02/1.78/10 <sup>b</sup>	15

**Table 1.** Cont.

Compound	Molecular Composition	Element Ratio	Hydration Water [mol/mol-POM]
NaPV <sub>2</sub> W	Na <sub>5</sub> [PV <sub>2</sub> W <sub>10</sub> O <sub>40</sub> ]	Na/P/V/W 6.52 <sup>b</sup> /1.21 <sup>b</sup> /2.31 <sup>b</sup> /10 <sup>b</sup>	14
HPV <sub>3</sub> Mo	H <sub>6</sub> [PV <sub>3</sub> Mo <sub>9</sub> O <sub>40</sub> ]	P/V/Mo 1.10 <sup>a</sup> /3.03/9	15
NaPV <sub>3</sub> W	Na <sub>6</sub> [PV <sub>3</sub> W <sub>9</sub> O <sub>40</sub> ]	Na/P/V/W 7.12 <sup>b</sup> /1.17 <sup>b</sup> /3.32 <sup>b</sup> /9 <sup>b</sup>	13
HPV <sub>4</sub> Mo	H <sub>7</sub> [PV <sub>4</sub> Mo <sub>8</sub> O <sub>40</sub> ]	P/V/Mo 1.41 <sup>a</sup> /4.03/8	23
NaPV <sub>4</sub> W	Na <sub>7</sub> [PVW <sub>8</sub> O <sub>40</sub> ]	Na/P/V/W 6.62/1.17 <sup>b</sup> /4.11 <sup>b</sup> /8 <sup>b</sup>	11
HPV <sub>5</sub> Mo	H <sub>8</sub> [PV <sub>5</sub> Mo <sub>7</sub> O <sub>40</sub> ]	P/V/Mo 1.21 <sup>a</sup> /5.02/7	9
NaPV <sub>5</sub> W	Na <sub>8</sub> [PV <sub>5</sub> W <sub>7</sub> O <sub>40</sub> ]	Na/P/V/W 6.79/1.10 <sup>b</sup> /5.13 <sup>b</sup> /7 <sup>b</sup>	11
HPV <sub>6</sub> Mo	H <sub>9</sub> [PV <sub>6</sub> Mo <sub>6</sub> O <sub>40</sub> ]	P/V/Mo 1.28 <sup>a</sup> /6.11/6	11
NaPV <sub>6</sub> W	Na <sub>9</sub> [PV <sub>6</sub> W <sub>6</sub> O <sub>40</sub> ]	Na/P/V/W 6.71/1.05/6.15 <sup>b</sup> /6 <sup>b</sup>	13

The element ratios were determined using AAS or ICP-OES, the water content was determined by TGA. All results were normalised to the framework metal (molybdenum or tungsten). <sup>a</sup> H<sub>3</sub>PO<sub>4</sub> was used in a slight excess during synthesis, so a slightly higher P content is expected, due to phosphate impurities. <sup>b</sup> Tungsten values are determined systematically too low with the applied measurement method, so that the values for the other elements appear to be too high.

There is a tendency for the tungstates to have higher crystal water contents than the molybdates, which can be correlated with the size of W(VI) compared to Mo(VI), since W(VI) is thus able to coordinate more hydrate water molecules.

The integrity and the characterization in the solid-state of all investigated Keggin-type structures was performed by ATR-FT-IR and Raman spectroscopy. Figure 1 shows the IR spectra of the POMs NaPV<sub>x</sub>W with  $x = 1$  to 6, and a comparison between  $x = 2$  for NaPV<sub>2</sub>W, HPV<sub>2</sub>W, and HPV<sub>2</sub>Mo is shown in Figure 2. IR spectra of the POMs HPV<sub>x</sub>Mo with  $x = 1$  to 6, and a comparison between the POMs with  $x = 1$  for NaPVW, HPVW, and HPVMo, can be found in Figures S1 and S2 in the Supplementary Materials.

IR spectroscopy of Keggin-type POMs, represents a common method for verifying the structure type and has been discussed extensively in the literature [23,32,33]. In general, the trend is evident that the IR bands are broadened with increasing degree of substitution. This observation correlates with the fact that more positional isomers are generated with increasing degree of substitution. The more isomers there are, the broader the bands become overall. The importance of the positional isomers for the evaluation of the further analysis is discussed in detail in the section on NMR spectroscopy. In particular, the assignment of the individual signals to the vibration modes is known from the literature, and has already been substantiated by numerous theoretical simulations. The work of Bridgeman (2004) [32], presents a computational study in which IR and Raman bands were predicted for the different Keggin isomers and compared to the real measured data [32]. In agreement with the literature, the present IR spectra show characteristic bands of a Keggin structure type. All observed vibrational bands were assigned to the corresponding vibration modes, according to Lee et al. [33]. The bands in the region of  $>1000\text{ cm}^{-1}$ , correspond to the phosphorus–oxygen vibration mode P–O, while the vibrational bands in the region between 950 and  $1000\text{ cm}^{-1}$  belong to the vibration modes of the terminal metal–oxygen bonds M = O<sub>t</sub>. In the region between 850 and  $900\text{ cm}^{-1}$  and in the region below  $800\text{ cm}^{-1}$ , the

vibrational bands of the metal–metal bridging oxygen–metal bonds can be located for the corner- ( $M-O-M$ )<sub>vertex</sub> and the edge- ( $M-O-M$ )<sub>edge</sub> linked octahedrons [23,32,33].

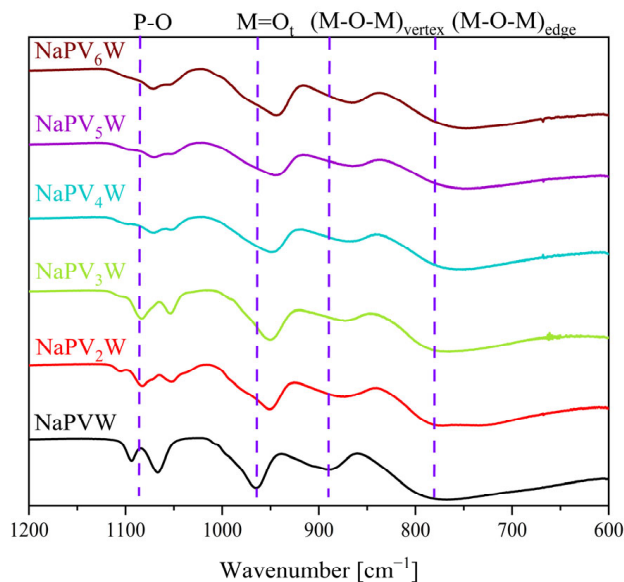


**Figure 1.** ATR-FT-IR spectra of the POMs  $NaPV_xW$ , with  $x = 1$  to 6.

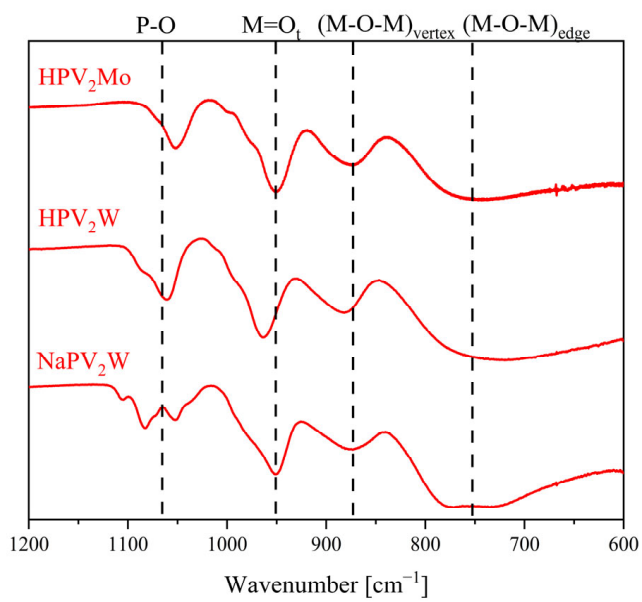


**Figure 2.** ATR-FT-IR spectra of the POMs  $NaPV_2W$ ,  $HPV_2W$ , and  $HPV_2Mo$ .

As the W(VI) positions are increasingly substituted with V(V) atoms of significantly lower mass, the vibrational bands shift to lower wavenumbers, since the corresponding vibration is more easily excited. This effect is already well reported in the literature for various substituted Keggin POMs [23,32,33]. The same trend is also observed for the Keggin-type molybdate series, but the effect is much more significant for the tungstates, due to the larger mass difference between W(VI) and V(V). In contrast to the molybdates, it is noticeable for the tungstates that the P–O vibrational band appears in two bands: the reason for this is the very same effect, although in this case the shift is sufficiently large to form a separate vibrational band. A closer look at the Keggin structure, reveals that the four oxygen atoms coordinating the central phosphorus atom tetrahedrally, are each part of an  $M_3O_{13}$  unit [34]. Thus, at higher wavenumbers, the vibrational band of the P–O mode

tends to originate from the P–O bond to whose oxygen atom a W(VI) rich  $W_3O_{13}$  unit is attached, while at lower wavenumbers the bands can be assigned to corresponding P–O vibrational bands of V(V) rich  $M_3O_{13}$  units.

The integrity of the Keggin structure has also been confirmed for the extracted heteropolyacids HPVW and  $HPV_2W$  (Figure 2 and Figure S2 Supplementary Materials). Here, the P–O band for the hetero-polyacid  $HPV_2W$  in Figure 2 is not split like that of  $NaPV_2W$ , which can be attributed to the V(V) loss during extraction (vide supra).

Table 2 illustrates the discussed trend, that the vibration bands for both the Keggin-type tungstates and respective molybdates shift to smaller wavenumbers with increasing degree of substitution. For the comparison between the V(V)-substituted tungstates and molybdates, the trend, especially for the degrees of substitution  $x = 1$  to 3, is that for the same degree of substitution, the vibrational bands of the tungstates are shifted to higher wavenumbers. This trend is due to the higher mass of the element tungsten, so that the corresponding vibrational modes require more energy to be excited. The same trends can also be seen when comparing the IR data of the unsubstituted parent POMs, HPMo and HPW (Figure S3, Supplementary Materials).

**Table 2.** Positions of the characteristic vibration bands of all POMs investigated in this work.

POM/Vibration Mode	P–O	$M = O_t$	$(M–O–M)_{\text{vertex}}$	$(M–O–M)_{\text{edge}}$
HPMo	1059	962	877	744
HPW	1073	973	904	756
$NaPVW$	1094, 1066	965	890	764
HPVW	1070	959	876	735
HPVMo	1055	955	872	729
$NaPV_2W$	1083, 1054	952	875	773
$HPV_2W$	1061	964	884	724
$HPV_2Mo$	1054	955	872	729
$NaPV_3W$	1084, 1054	950	876	765
$HPV_3Mo$	1053	954	877	730
$NaPV_4W$	1072, 1053	948	868	756
$HPV_4Mo$	1048	951	871	720
$NaPV_5W$	1070, 1052	945	865	751
$HPV_5Mo$	1047	949	868	719
$NaPV_6W$	1071, 1059	944	868	748
$HPV_6Mo$	1051	949	874	710

The success of V(V) substitution into the Keggin-type phosphotungstate structure can also be verified by Raman spectroscopy. Figure 3 shows the Raman spectra of the POMs  $NaPV_xW$  ( $x = 1$  to 6), and Figure 4 a comparison between the POMs  $NaPV_2W$ ,  $HPV_2W$ , and  $HPV_2Mo$ . Raman spectra of the POMs  $HPV_xMo$ , with  $x = 1$  to 6, and a comparison between the POMs with  $x = 1$ , for  $NaPVW$ ,  $HPVW$ , and  $HPVMo$ , can be found in Figures S4 and S5 in the Supplementary Materials. Essentially, a Raman spectrum of a Keggin structure shows the various vibrational modes of the  $M = O_t$  bond in the region around  $1000 \text{ cm}^{-1}$ , and the various M–O–M vibrational modes, particularly pronounced in the region below  $400 \text{ cm}^{-1}$  [32]. The vibrational modes of the P–O bonds are not Raman active. The success of the substitution is evident in the  $M = O_t$  bands, which strongly change their shape due to the substitution, and, especially in the case of the tungstates, shift to smaller wavenumbers with increasing degree of substitution. Due to the smaller mass of V(V) in comparison to W(VI), an additional shoulder forms with increasing degree of V(V) substitution. This is

the same phenomenon discussed above, for the IR spectra. A direct comparison between HPMo and HPW can be found in Figure S6, Supplementary Materials. Here the intensities of the vibration bands of HPW are not as intense, in comparison to HPMo.

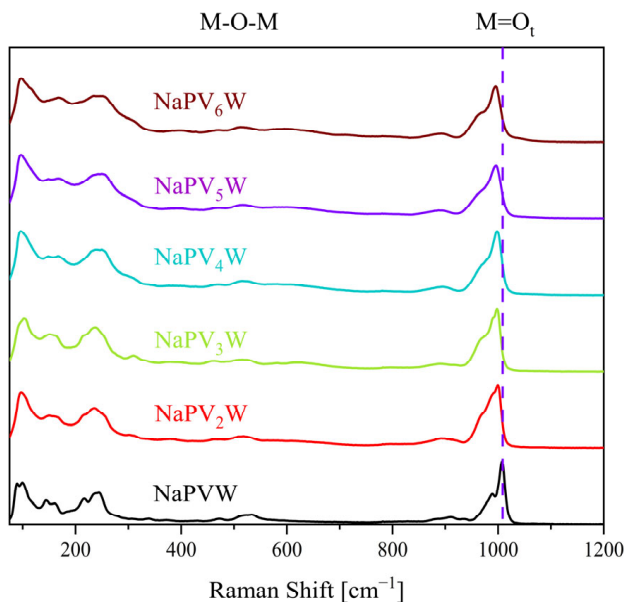


**Figure 3.** Raman spectra of the POMs  $\text{NaPV}_x\text{W}$ , with  $x = 1$  to 6. The purple line runs through the peak maximum of an  $\text{M} = \text{O}_t$  vibration band from  $\text{NaPVW}$ , to illustrate the trend of the peak shift dependence on the substitution degree.

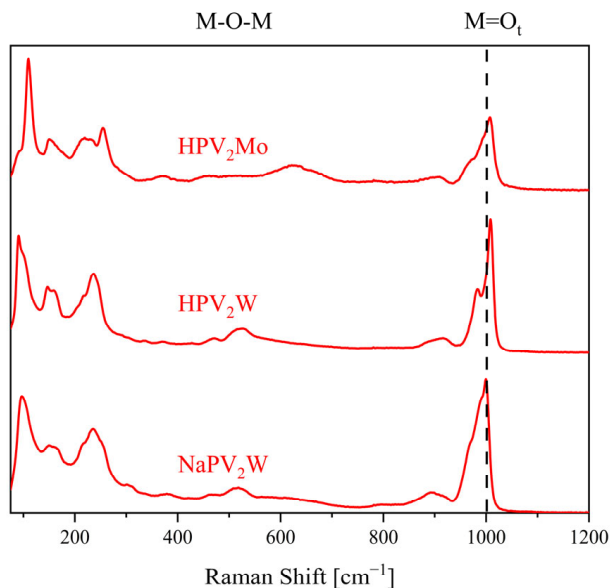


**Figure 4.** Raman spectra of the POMs  $\text{NaPV}_2\text{W}$ ,  $\text{HPV}_2\text{W}$ , and  $\text{HPV}_2\text{Mo}$ . The black line runs through the peak maximum of an  $\text{M} = \text{O}_t$  vibration band from  $\text{NaPV}_2\text{W}$ , to illustrate the trend of the peak shift dependence on the substitution degree.

To support our results from the solid-state characterization, we present two new single-crystal structures, of  $\text{NaPV}_5\text{W}$  in Figure 5 and Table 3, and  $\text{NaPV}_2\text{W}$  in Figure S7 (Supplementary Materials). The crystallographic information files (.cif) can be found in the CCDC database, with the deposition numbers: 2240685 ( $\text{NaPV}_2\text{W}$ ) and 2240686 ( $\text{NaPV}_5\text{W}$ ). Detailed refinement data are found in the Supplementary Materials, Section 2.9. All compounds were crystallised in the tetragonal space group  $\text{P}4/\text{mnc}$  (128) and grown by

slow evaporation of water from an aqueous POM solution, in a desiccator, under reduced pressure. Further information about the unit cell and the space groups can be found in Table S4, Supplementary Materials. The crystal structures show a distinct disorder of the central phosphorous atom. This is a known disorder type, which is found in many Keggin-type crystal structures (e.g., CCDC database deposition number: 1628559). As suggested by the disorder of the central  $\text{PO}_4$  tetrahedron, the phosphorus coordination appears cubic. However, it is a tetrahedral coordination, as can easily be seen if the four oxygen atoms are partially occupied (occupation 0.5). All metal atoms are in an octahedral coordination by six oxygen atoms, and have a terminal oxo ligand with double bond character, as can be seen from the shortened bond length (Table 3). All the crystallographic information of both structures is summarised in Table 3. To gain better insights into the obtained structures, the bond lengths are compared to the sum of covalent radii.

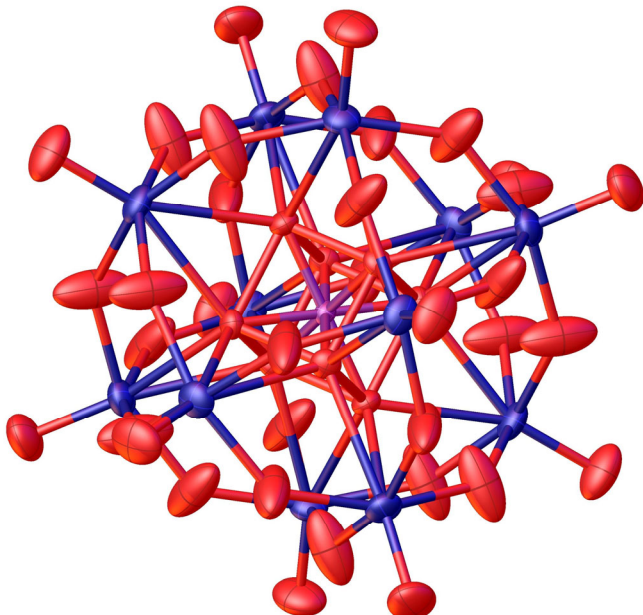


**Figure 5.** Solid-state structure of compound  $\text{NaPV}_5\text{W}$ , determined by X-ray diffraction. The compound was crystallised in the space group  $\text{P}4/\text{mnc}$  (128). Residual electron density attributed to hydration water has been refined with a solvent mask (SQUEEZE).  $R_1$ : 2.64%,  $wR_2$ : 6.46%,  $R_{\text{int}}$ : 5.86%, GooF: 1.032. Colour code: purple: phosphorous, red: oxygen, and blue: metals (W, V).

**Table 3.** Found bond lengths vs. weighted sum of covalent radii of the obtained single-crystal structures. Values for compound  $\text{HPV}_5\text{Mo}$  were taken from Poller et al. [35].

Bond Type	Found Bond Length [ $\text{\AA}$ ]			Weighted Sum of Covalent Radii [ $\text{\AA}$ ]	
	$\text{NaPV}_2\text{W}$	$\text{NaPV}_5\text{W}$	$\text{HPV}_5\text{Mo}$	$\text{NaPV}_2\text{W}$	$\text{NaPV}_5\text{W}$
P1–O1	1.532	1.540	1.540	1.740	1.740
O1–M1,2	2.445	2.416	2.400	1.995	1.988
M1,2–O2,3,4	1.887	1.870	1.919	1.995	1.988
M1,2=O5,6	1.653	1.649	1.635	1.995	1.988

$BL = \frac{a(r_O+r_W)+b(r_O+r_V)}{a+b}$ , with  $BL$  the weighted bond length,  $a$  and  $b$  the weighing factors, and  $r$  the covalent radii of the elements O, W, and V.

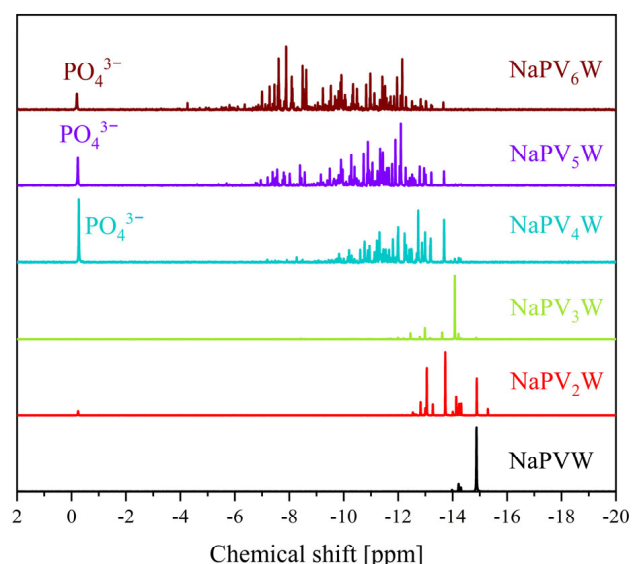
From Table S4 (Supplementary Materials) it is visible that the lattice parameters decrease with increasing substitution degree, due to the smaller size of V(V) in comparison to W(VI).

Table 3 verifies the trend that the bond lengths of  $\text{NaPV}_5\text{W}$  are shorter than those of  $\text{NaPV}_2\text{W}$ . By comparing the found bond lengths with those of the weighted sums of covalent radii, it is obvious that the found P–O bond length is shorter than the calculated value for the sum of the covalent radii, indicating a stronger nature of this bond. The four oxygen atoms coordinating the central phosphorus, link the phosphorus to the twelve metal atoms of the Keggin structure. This bond type is denoted O1–M1.2 in this work. As expected for a Keggin-type structure, the O1–M1.2 bond length is longer than the calculated values in Table S4, indicating a more coordinative bond nature [23]. The bond length of the M1,2–O2,3,4 bond, linking the metals together, is found to be minimally longer than the sum of the covalent radii. In contrast, the bond length M1,2=O5,6, proves to be significantly shortened, since this bond type is characterised by partial double bond character. A specific substitution pattern could not be identified in both structures, because the V(V) atoms are statistically distributed over the W(VI) positions. Therefore, the W(VI) positions were refined with a corresponding partial occupation by V(V), assuming a statistical distribution.

The solid-state structure of  $\text{NaPV}_5\text{W}$  was compared to our previous published structure of  $\text{HPV}_5\text{Mo}$ , in the work of Poller et al. [35]. This structure is also available in the CCDC database, with the deposition number: 2177881. By comparing the found bond lengths of this compound in Table S4, with those of  $\text{NaPV}_5\text{W}$ , it is obvious that the bond lengths of  $\text{NaPV}_5\text{W}$  tend to higher values, due to the larger ionic size of W(VI) in comparison to Mo(VI). Only, the M1,2–O2,3,4 bond length deviates from this trend.

Characterization of the POMs in aqueous solution was performed using NMR and UV-Vis spectroscopy. The behaviour of the phosphotungstates in aqueous solution was analysed by  $^{31}\text{P}$ - and  $^{51}\text{V}$ -NMR spectroscopy. For comparable pH conditions, the pH was adjusted to 1 using hydrochloric acid, additionally, approx. 10% of deuterated acetone was added, to enable the solvent lock. In our experience, the NMR spectra of the free acids  $\text{HPV}_x\text{Mo}$  ( $x = 1$  to 6) cannot be measured with deuterated water as the solvent. Due to the acidic free protons of the POM, the protons rapidly exchange against deuterium from  $\text{D}_2\text{O}$ , which causes the NMR lock to fail during the measurement.

Figures 6 and 7 show the  $^{31}\text{P}$  and  $^{51}\text{V}$  NMR spectra of the  $\text{NaPV}_x\text{W}$  POMs, with  $x = 1$  to 6, and Figures 8 and 9 the  $^{31}\text{P}$ - and  $^{51}\text{V}$ -NMR spectra of a comparison between  $\text{NaPV}_2\text{W}$ ,  $\text{HPV}_2\text{W}$ , and  $\text{HPV}_2\text{Mo}$ . Spectra of the POMs  $\text{HPV}_x\text{Mo}$ , with  $x = 1$  to 6, are shown in Figures S8 and S9, together with a  $^{31}\text{P}$ - and  $^{51}\text{V}$ -NMR comparison for the POMs  $\text{NaPVW}$ ,  $\text{HPVW}$ , and  $\text{HPVMo}$ , in Figures S10 and S11 in the Supplementary Materials.



**Figure 6.**  $^{31}\text{P}$ -NMR spectra of the POMs  $\text{NaPV}_x\text{W}$ , with  $x = 1$  to 6. All spectra were measured in a mixture of 70% water (pH 1) and 30%  $\text{D}_2\text{O}$ . Measurement frequency: 242.9 MHz; 85%  $\text{H}_3\text{PO}_4$  was used as an external standard.

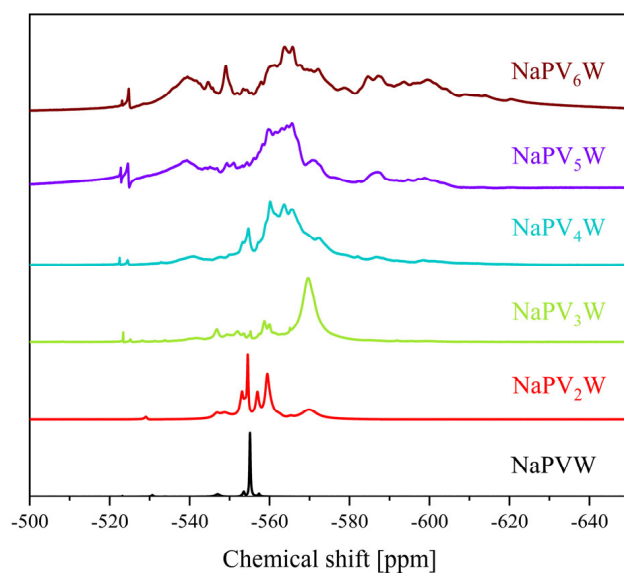


**Figure 7.**  $^{51}\text{V}$ -NMR spectra of the POMs  $\text{NaPV}_x\text{W}$ , with  $x = 1$  to 6. All spectra were measured in a mixture of 70% water (pH 1) and 30%  $\text{D}_2\text{O}$ . Measurement frequency: 157.8 MHz;  $\text{NaVO}_3$  was used as an external standard.

All peaks for the V(V)-substituted POMs, appear in the  $^{31}\text{P}$ -NMR spectra in the range between  $-5$  and  $-2$  ppm for  $\text{HPV}_x\text{Mo}$ , and in the range between  $-15$  and  $-6$  ppm for  $\text{NaPV}_x\text{W}$ . This means that the phosphorus atom is significantly more shielded by the increased electron density of the tungstate atoms, compared to the molybdenum atoms. The intense peak around 0 ppm can be attributed to free phosphate,  $\text{PO}_4^{3-}$ , resulting from different, pH-dependent dissociation equilibria. In the  $^{51}\text{V}$ -NMR spectra, the peaks appear in the range between  $-520$  and  $-610$  ppm. The difference in chemical shifts for  $\text{HPV}_x\text{Mo}$  and  $\text{NaPV}_x\text{W}$  is not as significant as in the  $^{31}\text{P}$ -NMR spectra. However, the  $^{51}\text{V}$  chemical shifts for  $\text{NaPV}_x\text{W}$  also tend to lower values. The more V(V) substituted the tungstate, the more positive the  $^{31}\text{P}$  chemical shifts tend to be, since the V(V) has significantly fewer electrons than the W(VI), resulting in a deshielding effect.

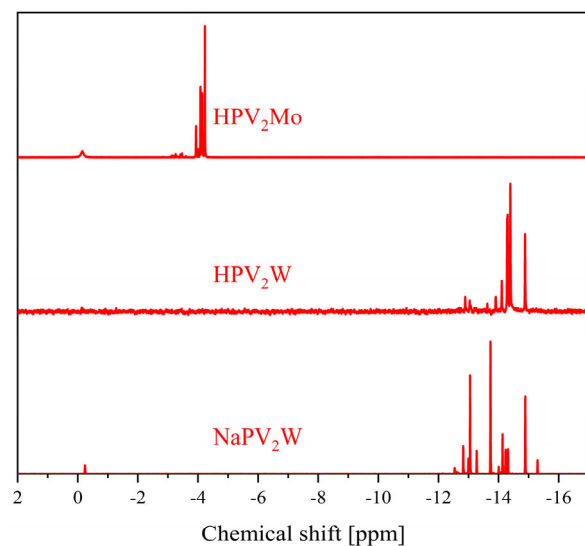


**Figure 8.**  $^{31}\text{P}$ -NMR spectra of the POMs  $\text{NaPV}_2\text{W}$ ,  $\text{HPV}_2\text{W}$ , and  $\text{HPV}_2\text{Mo}$ . Spectra for  $\text{NaPV}_2\text{W}$  and  $\text{HPV}_2\text{W}$  were measured in a mixture of 70% water (pH 1) and 30%  $\text{D}_2\text{O}$ , and spectra for  $\text{HPV}_2\text{Mo}$  were measured in a mixture of 90% water (pH 1) and 10% acetone- $d_6$ . Measurement frequency: 242.9 MHz; 85%  $\text{H}_3\text{PO}_4$  was used as an external standard.

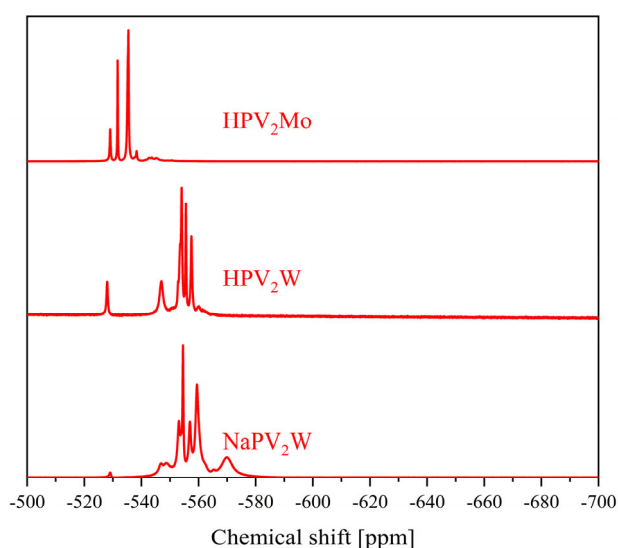


**Figure 9.**  $^{51}\text{V}$ -NMR spectra of the POMs  $\text{NaPV}_2\text{W}$ ,  $\text{HPV}_2\text{W}$ , and  $\text{HPV}_2\text{Mo}$ . Spectra for  $\text{NaPV}_2\text{W}$  and  $\text{HPV}_2\text{W}$  were measured in a mixture of 70% water (pH 1) and 30%  $\text{D}_2\text{O}$ , and spectra for  $\text{HPV}_2\text{Mo}$  were measured in a mixture of 90% water (pH 1) and 10% acetone- $d_6$ . Measurement frequency: 157.8 MHz;  $\text{NaVO}_3$  was used as an external standard.

For the respective mono-substituted molybdates and tungstates, only one peak appears in both spectra: For the two-fold and higher substituted POMs, several signals appear in the  $^{31}\text{P}$ - and  $^{51}\text{V}$ -NMR spectra. This effect has already been discussed to a great extent in the literature for V(V), as well as Mn(II)/V(V)-substituted phosphomolybdates [23,36–38]. Once two framework metals are replaced by V(V), a total of five positional isomers are possible, so that a corresponding number of peaks can be identified in the NMR spectra. The more framework metals are replaced with V(V), the more positional isomers are possible, resulting in more NMR signals being observed. This trend is a result of there already being 27 position isomers for a substitution degree of  $x = 4$ , 38 for  $x = 5$ , and 48 for  $x = 6$  [36]. This leads to an increase in the complexity of the NMR spectra. Therefore, it is easy to see that, especially for the more highly substituted molybdates and tungstates, with degrees of substitution of  $x > 3$ , multiple signals are found in the  $^{31}\text{P}$  and  $^{51}\text{V}$  data [37,38]. In particular, the  $^{51}\text{V}$ -NMR shifts of the individual positional isomers are very similar, so that they merge into broad peaks, especially for the highly substituted analogues [23,36–38]. The positional isomers addressed, can be primarily assigned to  $\alpha$  Keggin isomers: In addition to the positional isomerism, it must be considered that there are different structural isomer types of a Keggin structure, namely the  $\alpha$  and the  $\beta$  type [39–41]. Two  $\text{MO}_6$  octahedra can be connected by common edges and corners. The edge connection is the energetically less favourable variant, due to the increased Coulomb repulsion compared to the corner connection. Depending on which edges the octahedra share, the M–M–M angle can be 60, 90, 120, or 180°, with the 60° arrangement being energetically favoured. Thus, the arrangement of the four  $\text{M}_3\text{O}_{13}$  triads with the 60° M–M–M angle, with the octahedra linked by common corners, represents the geometry with the minimum Coulomb repulsion. This geometry is therefore also called the corresponding  $\alpha$  isomer of the Keggin structure. The  $\beta$  isomer is obtained by rotating an  $\text{M}_3\text{O}_{13}$  triad by 60° of a three-fold axis of the  $\alpha$  isomer, and represents the energetically less favourable isomer [39]. Even though the  $\alpha$  isomer is energetically preferred, formation of the  $\beta$  isomer, along with corresponding  $\beta$  positional isomers, still occurs, increasing the complexity of the NMR spectra. However, the  $\beta$  Keggin isomers play a minor role compared to the  $\alpha$  isomers, due to their higher instability, so that  $\beta$  isomer peaks are mainly expressed by low intensity signals in the NMR spectra. This can explain the peaks with low intensities, especially in the  $^{31}\text{P}$ -NMR spectra. Thus, the lower intensity peak at  $\sim 14$  ppm in the  $^{31}\text{P}$ -NMR for  $\text{NaPVW}$ , can be assigned

to a  $\beta$  isomer of the Keggin structure, while the high intensity peak at  $-15.3$  ppm, belongs to the corresponding  $\alpha$  isomer [37,38,42].

For all POM species, different dissociation equilibria are found in aqueous acidic media [23]. This means that the complexity of the spectra is further increased, in addition to the positional and structural isomer ( $\alpha/\beta$ ) peaks.

It is known from the previous state of the literature, that the stability of the Keggin-type structures decreases with an increasing degree of substitution, which means that the maximum of substitution is the half of all framework metals ( $x = 6$ ) [20–22]. Although the representatives with the degree of substitution  $x = 6$  are sufficiently stable for many applications, the observed trend means only that Keggin structures with a degree of substitution of  $x > 6$  are not synthetically accessible using our presented methods. Possible reasons for this observation are, the increasing anionic charge and basicity, since hexavalent metals are replaced by pentavalent ones. The anionic charge of the scaffold, on the other hand, always remains constant, due to the 40 oxygen atoms in oxidation state -II, which means that the total charge of the final Keggin anions must increase with increasing  $x$ . At some point, an anionic charge is exceeded (for  $x = 6$ , the anionic charge is 9), from which a POM anion can no longer be stabilised, since too much anionic charge meets too little surface or volume in a defined size of a Keggin-type cluster. In the  $^{31}\text{P}$ - and  $^{51}\text{V}$ -NMR spectra, this is reflected in the trend that, in addition to the isomer peaks, more dissociation peaks occur for higher  $x$ . Thus, the species with  $x = 1$  also have only one peak each in the respective NMR spectra, since the dissociation in solution takes place only to a minor extent, due to the comparatively high POM stability. More than five peaks are already found for  $x = 2$ , suggesting an increased dissociation tendency. Thus, the more highly substituted POMs, especially those with  $x > 3$ , no longer have only 27, 38, or 48 signals, so the spectra show an increasing number of dissociation signals. Thus, the trend is also reflected in the increasingly complex NMR spectra in aqueous solution [36].

The extent of dissociation is strongly dependent on the pH value of the solution. A dissociation of the POM can take place, with the release of pervanadyl cations  $\text{VO}_2^+$  and the corresponding lacunary species, according to  $[\text{PV}_x\text{M}_{12-x}\text{O}_{40}]^{(3+x)-} \rightarrow n \text{VO}_2^+ + [\text{PV}_{x-n}\text{M}_{12-x}\text{O}_{40}]^{(3+x+n-5)-}$  [43]. The formation of lower or higher substituted analogues has also been discussed in the literature, according to  $2 [\text{PV}_x\text{M}_{12-x}\text{O}_{40}]^{(3+x)-} \rightarrow [\text{PV}_{x+1}\text{M}_{11-x-1}\text{O}_{40}]^{(3+x+1)-} + [\text{PV}_{x-1}\text{M}_{12-x+1}\text{O}_{40}]^{(3+x-1)-}$  [23,43]. Thus, the dissociation equilibria also contribute to the fact that different NMR signals can be observed. For example, a  $\text{VO}_2^+$  cation is visible in the  $^{51}\text{V}$ -NMR spectra, with a broad peak around  $-545$  ppm [23,43]. Overall, this means that the POM solution contains a statistical mixture of differently substituted species. E.g., a sample of HPVMo would show a statistical distribution between HPMo/HPVMo/HPV<sub>2</sub>Mo.

A comparison of the  $^{31}\text{P}$  data between HPMo and HPW, is shown in Figure S12, Supplementary Materials. Here, the trend becomes visible that the  $^{31}\text{P}$  peak of HPW appears at lower chemical shifts. As expected, only one signal is observed for both POMs. Table 4 shows an overview of the different chemical shifts of all of the POMs investigated in this work.

**Table 4.**  $^{31}\text{P}$  and  $^{51}\text{V}$  chemical shifts of the POMs investigated in this work.

Substitution Degree	Molybdates		Tungstates	
	$^{31}\text{P}$ Shift [ppm]	$^{51}\text{V}$ Shift [ppm]	$^{31}\text{P}$ Shift [ppm]	$^{51}\text{V}$ Shift [ppm]
0	-3.75	-	-15.3	-
1	-4.22	-531.6	-14.9	-555.1
2	-3.94, -4.00, -4.08, -4.14, -4.23	-529.0, -531.7, -535.4, -538.3	-12.8 to -14.9	-538.5 to -578.8

**Table 4.** Cont.

Substitution Degree	Molybdates		Tungstates	
	$^{31}\text{P}$ Shift [ppm]	$^{51}\text{V}$ Shift [ppm]	$^{31}\text{P}$ Shift [ppm]	$^{51}\text{V}$ Shift [ppm]
3	−3.15 to −3.64 and −3.98 to −4.23	−526.4, −531.6, −534.0, −534.7, −537.2, −540.2 to −549.7	−11.6 to −15.0	−519.5 to −589.7
4	−2.47 to −4.24	−531.2 to −554.4	−9.1 to −14.5	−519.0 to −623.6
5	−1.00 to −4.25	−490.0 to −610.0	−6.4 to −14.2	−519.0 to −617.9
6	−1.50 to −4.50	−500.0 to −590.0	−6.6 to −14.2	−520.2 to −640.8

In order to obtain deeper insights into the properties of the POMs in solution, UV-Vis measurements were carried out. Table 5 shows a list of the observed peaks, which have been attributed to the ligand-to-metal charge transfer (LMCT) bands of the POMs [23,44–48]. The corresponding spectra are shown in Figures S13–S17 in the Supplementary Materials. For the V(V)-substituted POMs, two LMCT bands appear in the UV-Vis spectrum: an LMCT band for the Mo(VI)/W(VI) at shorter wavelengths, and a band for V(V) at longer wavelengths. For the V(V) phosphomolybdates, it is known that the LMCT bands of Mo(VI) and V(V) have a shoulder towards higher wavelengths. The band at shorter wavelengths is assigned to the LMCT of  $\text{M} = \text{O}_t$  (transition from the terminal oxygen atom to the metal), and the band causing the shoulder can be assigned to the LMCT of  $\text{M}-\text{O}_b/\text{M}-\text{O}_c$  (transition from the bridging oxygen atoms to the metal) [23,47,48]. Figures S13 and S14 in the Supplementary Materials show a plot of the corresponding LMCT wavelength positions against the POMs, for the  $\text{NaPV}_x\text{W}$  and  $\text{HPV}_x\text{Mo}$ , with  $x = 1$  to 6. For the  $\text{NaPV}_x\text{W}$  POMs, only the LMCT of W(VI) can be clearly identified at wavelengths above the LMCT bands of Mo(VI). The LMCT band of V(V) on the other side cannot be identified in the spectra, for the degrees of substitution  $x = 1$  to 3, even at elevated concentrations. Only at substitution degrees  $x > 3$ , can the LMCT for V(V) be observed, as an extremely broad band to which no clear peak maximum can be assigned. Thus, the spectra of the tungstates clearly differ from those of the molybdates. The peak positions of the LMCTs in Table 5 and Figures S13 and S14, clearly show the LMCTs for Mo(VI) in the range of 211 to 218 nm, while the LMCTs for W(VI) are in the range of 234 to 260 nm [26]. In general, the LMCT bands for W(VI) are shifted to higher wavelengths in comparison to Mo(VI), which indicates a smaller HOMO–LUMO gap in the tungstates. The LMCT bands for V(V) in the molybdates are found above 300 nm, in the range of 304 to 309 nm, in the case of the tungstates, the  $\text{O} \rightarrow \text{V(V)}$  LMCT bands are very broad, in the range of 330 to 400 nm, which makes it impossible to determine the exact maximum. For the three LMCT  $\lambda$  bands, the following trend can be concluded:  $\lambda_{\text{Mo(VI)}} < \lambda_{\text{W(VI)}} < \lambda_{\text{V(V)}}$ .

**Table 5.** Peak positions of the LMCT determined for the molybdates and tungstates.

POM/LMCT	$\text{O} \rightarrow \text{M(VI)}$ ( $\text{M} = \text{Mo, W}$ )	$\text{O} \rightarrow \text{V(V)}$
HPMo	214.0	-
HPW	255.5	-
HPV <sub>1</sub> Mo	211.5	308.5
HPV <sub>2</sub> Mo	214.5	308.0
HPV <sub>3</sub> Mo	215.0	305.0
HPV <sub>4</sub> Mo	218.0	304.0
HPV <sub>5</sub> Mo	217.0	308.0

**Table 5.** Cont.

POM/LMCT	$O \rightarrow M(VI)$ ( $M = Mo, W$ )	$O \rightarrow V(V)$
HPV <sub>6</sub> Mo	217.0	308.0
NaPVW	260.0	*
NaPV <sub>2</sub> W	242.0	*
NaPV <sub>3</sub> W	250.0	*
NaPV <sub>4</sub> W	240.0	*
NaPV <sub>5</sub> W	235.0	*
NaPV <sub>6</sub> W	234.0	*

\* For the tungstates, the LMCT for V(V) cannot be reliably determined because of the peak width.

By looking at the UV-Vis spectra of the molybdates and tungstates in Figures S15 and S16 (Supplementary Materials), it is noticeable that, at the same concentration measured, the intensities of the LMCT bands for Mo(VI)/W(VI) decrease with increasing degree of substitution, while the intensities of the bands for the LMCT V(V) increase with increasing degree of substitution. This observation correlates with the Mo(VI)/W(VI)/V(V) content in the POMs, and can therefore be interpreted as an indicator of successful substitution [23,47,48].

For both POMs HPMo and HPW, only one LMCT band is visible in the UV-Vis spectra (Figure S19, Supplementary Materials), assigned to the LMCT bands of Mo(VI) and W(VI).

The LMCT peak maxima were analysed according to the Beer-Lambert law, and the extinction coefficients,  $\epsilon_\lambda$ , were determined for each LMCT wavelength (Equation (1), Supplementary Materials). For this purpose, stock solutions of the POMs were first prepared, at a concentration of 1 g/L, which were then diluted in a dilution series to five different concentrations, used to construct the calibration curve (Equation (2), Supplementary Materials). The slope of the linear function can then be used to calculate the extinction coefficient for a defined wavelength (Equations (3) and (4)), Supplementary Materials). In this way, knowing the previously determined calibration lines, the extinction coefficients were calculated, and are summarised in Table 6. Figure 10 shows a plot of the extinction coefficients against the degree of substitution, for the molybdates and tungstates. All calibration lines can be found in the Supplementary Materials in Figures S20–S37.

**Table 6.** Extinction coefficients,  $\epsilon_\lambda$ , calculated for the different LMCT wavelengths.

Substitution Degree, $x$	HPV <sub>x</sub> Mo		NaPV <sub>x</sub> W
	Mo(V) [L mol <sup>-1</sup> cm <sup>-1</sup> ]	V(V) [L mol <sup>-1</sup> cm <sup>-1</sup> ]	W(VI) [L mol <sup>-1</sup> cm <sup>-1</sup> ]
1	88,247	18,705	36,532
2	88,289	21,140	33,402
3	74,813	17,004	37,975
4	66,427	16,526	41,484
5	81,571	20,115	46,798
6	76,012	18,094	39,371

For consideration of Figure 10, it is important to note that the extinction coefficients determined for the V(V) LMCT are from the molybdates data. For the tungstates, the extinction coefficient for the V(V) LMCT could not be calculated, because the wavelength of the LMCT maxima could not be accurately determined in this case. Discussing the results in Table 6 and Figure 10, it is striking that the extinction coefficients for the V(V) LMCT are in the range of  $1.6\text{--}2.1 \times 10^4$  L mol<sup>-1</sup> cm<sup>-1</sup>, while the extinction coefficients for the W(VI) LMCT are in the range of  $3.3\text{--}4.6 \times 10^4$  L mol<sup>-1</sup> cm<sup>-1</sup>. The extinction coefficients for the

Mo(VI) LMCT bands show the highest values, in the range of  $6.6\text{--}8.8 \times 10^4 \text{ L mol}^{-1} \text{ cm}^{-1}$ . So, the following trend can be concluded:  $\varepsilon_{\lambda}^{\text{V(V)}} < \varepsilon_{\lambda}^{\text{W(VI)}} < \varepsilon_{\lambda}^{\text{Mo(VI)}}$ .

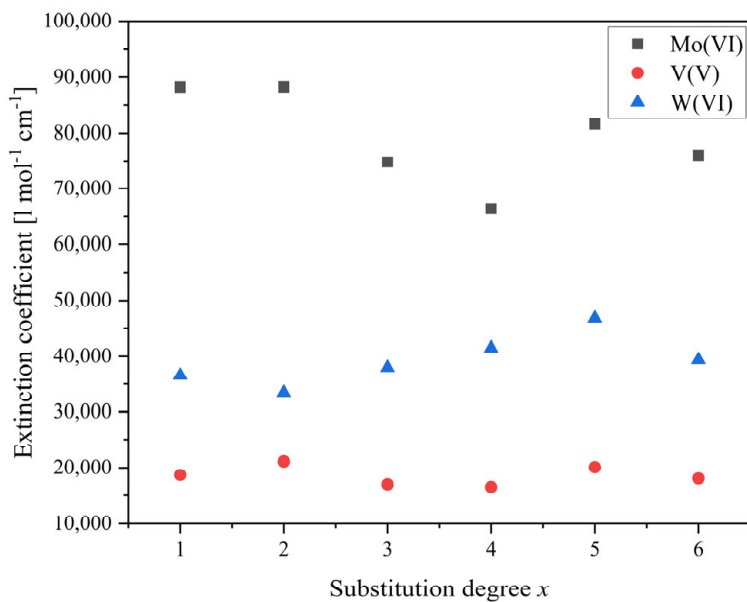


**Figure 10.** Plot of the extinction coefficients versus substitution degree.

The knowledge of the respective extinction coefficients proves to be particularly useful for different applications, e.g., in homogeneous catalysis. A problem with homogeneously based catalysts, is the difficult separation of the products from the product phase and the complete removal of the catalyst. Thus, by knowing the extinction coefficient, conclusions can be drawn about the remaining residual concentration of the POM in the purified product phases, using photometry. This conclusion can also be applied with regard to bio-based applications. Here, too, a photometric determination of the concentration of the POM can help to make a study successful.

Figures 11 and 12 show pictures of the different molybdate and tungstate solutions (concentration 1 g/L), with increasing degree of substitution from left to right. The higher the substitution degree, the more intense is the red colour of the POM solution, starting from yellow ( $x = 1$ ) up to red ( $x = 6$ ).



**Figure 11.** Solutions (1 g/L) of the different V(V)-substituted molybdates, with increasing degree of substitution from left to right,  $x = 1\text{--}6$ .



**Figure 12.** Solutions (1 g/L) of the different V(V)-substituted tungstates, with increasing degree of substitution from left to right,  $x = 1\text{--}6$ .

The redox potentials of the molybdates and tungstates were measured using CV and SWV. Our method worked at a pH of 1, which was previously adjusted with hydrochloric acid. This corresponds to a hydrogen ion concentration of 0.1 mol/L. The analyte concentration was 1 mmol/L. Thus, a ratio of electrolyte to analyte of 100:1 was used. All CV data can be found in the Supplementary Materials in Figures S38–S46, together with a tabular overview of the peak potential maxima, minima, and mean values from the CV data, and the maxima from the SWV data (Table S1, Supplementary Materials). The resolution of the CV data remains poor, since the various peak potentials partially overlap, especially for the molybdates. Figures 13 and 14 show the SWV data of the POMs  $\text{NaPV}_x\text{W}$ , with  $x = 1$  to 6, and a comparison between the POMs  $\text{NaPV}_2\text{W}$ ,  $\text{HPV}_2\text{W}$ , and  $\text{HPV}_2\text{Mo}$ . SWV data of the POMs  $\text{HPV}_x\text{Mo}$ , with  $x = 1$  to 6, and a comparison between the POMs  $\text{NaPVW}$ ,  $\text{HPVW}$ , and  $\text{HPVMo}$ , are available in the Supplementary Materials, in Figures S42–S44.

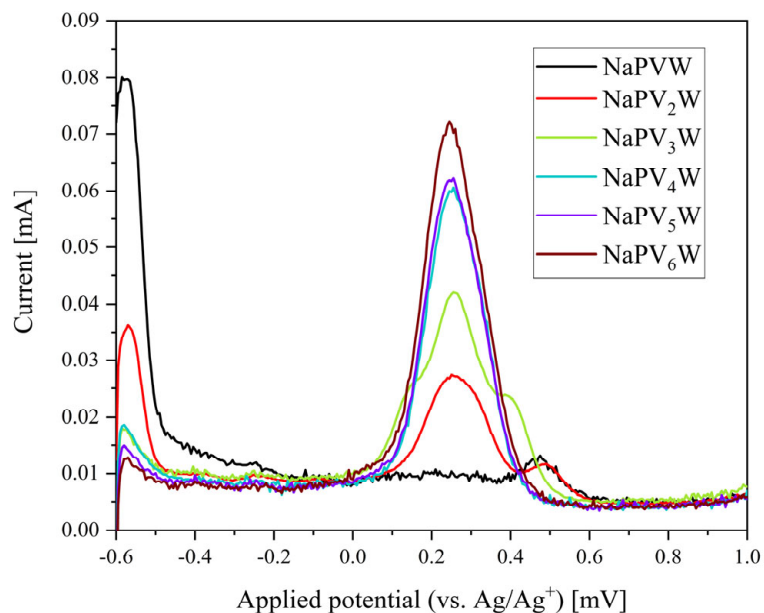


**Figure 13.** SWV data of the POMs  $\text{NaPV}_x\text{W}$ , with  $x = 1$  to 6 (concentration 1 mmol/L, scan rate 5 mV and pH 1 (HCl as supporting electrolyte)).

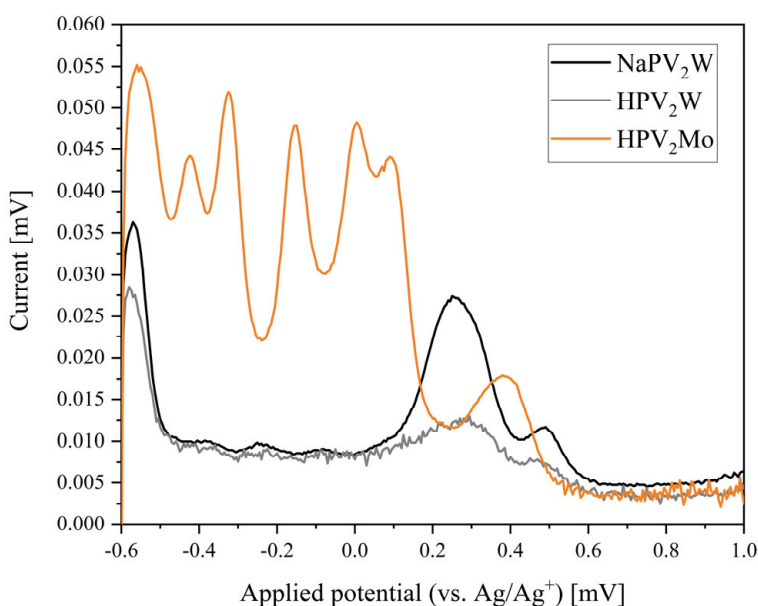


**Figure 14.** SWV data of the POMs  $\text{NaPV}_2\text{W}$ ,  $\text{HPV}_2\text{W}$ , and  $\text{HPV}_2\text{Mo}$  (concentration 1 mmol/L, scan rate 5 mV and pH 1 (HCl as supporting electrolyte)).

The different redox behaviour of the tungstates in comparison to the molybdates, is already visible by comparing the CV and SWV data of the unsubstituted HPMo and HPW, in Figures S45 and S46. In the SWV data (Figure S46), six redox processes are observed for HPMo, whereas only two redox processes were detected for HPW.

Similarly, when comparing the CV and SWV data of the molybdates and tungstates (Figure 13 and Figure S38–S43), the molybdates generally show seven to eight redox processes, while only two to three redox processes are observed for the tungstates. This means that the redox chemistry of the tungstates is limited compared to the molybdates. In the SWV data of the substituted tungstates (Figure 13), mainly a broad peak potential in the range between 100 and 400 mV is recognizable, whose intensity increases with increasing degree of substitution. It is known from the literature, that the peak potentials of the molybdates are the result of numerous two-electron redox reactions, while for the tungstates mainly one-electron redox reactions are observed [23,26,49–51]. The substitution of the molybdate or tungstate framework with V(V), changes the entire electronic structure of the POM, which also changes the electrochemical potentials [23]. This observation is particularly evident for the substituted molybdates. The electrochemical process observed for the POMs  $\text{HPV}_x\text{Mo}$  ( $x = 1$  to 3) at  $\sim 70$  mV, likely originates from the  $\text{VO}_2^+$  cation dissociating from the POM structure in the aqueous acidic media [23,43]. Especially noteworthy, is the shift of this potential to higher voltages, depending on the degree of substitution, starting from 70 mV for HPVMo, over 90 mV for  $\text{HPV}_2\text{Mo}$ , to 95 mV for  $\text{HPV}_3\text{Mo}$  (Figure S42, Supplementary Materials). Starting from a degree of substitution of  $x = 4$ , this peak eventually merges with the peak in the range between  $-200$  and  $-100$  mV and 0 to 200 mV. This results in a broad signal in the range between  $-200$  and 200 mV, in which the individual electrochemical potential for the  $\text{VO}_2^+$  cation can no longer be identified (Figure S43, Supplementary Materials). In general, the other potentials of the substituted molybdates are also subject to a shift, with a trend toward shifting maxima (see Figure S42, Supplementary Materials) to larger potential values, particularly for the potentials below  $-400$  mV. Thus, the V(V) substitution can be seen here as a tool for selective tailoring of the redox activity of a POM to a desired application [23]. This is particularly evident from the fact that, very low redox activity of the POM is observed in the case of the V(V)-substituted tungstates.

The electrochemical results suggest a significantly lower redox activity of the tungstates. It can therefore be concluded that for further redox applications (in catalysis or in biomedicine),

V(V)-substituted molybdates should be preferred instead of tungstates, since their redox activity is much more pronounced.

### 3. Materials and Methods

#### 3.1. Chemicals

All chemicals used were purchased from common suppliers of research chemicals. A detailed list is provided in the Supplementary Materials.

#### 3.2. Experimental

Detailed descriptions and additional data can be found in the Supplementary Materials.

#### 3.3. Synthesis of $H_{3+x} [PV_x Mo_{12-x} O_{40}]$ , according to Odyakov et al. [20–22]

##### Step 1:

Molybdenum trioxide was suspended in deionised water and a 25% phosphoric acid solution in water was added. It was heated to reflux, wherein a clear yellow solution was formed.

##### Step 2:

Parallel to step 1, divanadium pentoxide was suspended in water and cooled to 0 °C. While stirring, a 30% hydrogen peroxide solution in water was added dropwise. Thereby, the divanadium pentoxide began to dissolve in the form of a red/brown solution and the release of oxygen gas was observed. After the divanadium pentoxide was completely dissolved, a 25% phosphoric acid solution in water was added to the batch, and stirred at room temperature.

The vanadium solution from step 2 was added dropwise to the refluxing molybdenum solution from step 1. It was further refluxed for 60 min and then cooled to room temperature. The solution was filtered and concentrated under reduced pressure. A red or dark brown solid was obtained.

#### 3.4. Synthesis of $Na_{9-x} H_x [PW_9 O_{34}]$ , according to Domaille et al. [29]

The lacunary species  $Na_{9-x} H_x [PW_9 O_{34}]$ , was synthesised according to Domaille et al. [29], starting from sodium tungstate dihydrate and phosphoric acid.

Sodium tungstate dihydrate was dissolved in deionised water and a 85% phosphoric acid solution in water was added. The final pH value was adjusted to 8.9. While stirring, glacial acetic acid was added dropwise, and during addition a colourless precipitate was formed. The pH changed to 7.4 after complete addition. After two hours of stirring, the colourless precipitate was removed by vacuum filtration and was dried in a desiccator for 24 h. The product was used without further purification. A colourless solid was obtained.

#### 3.5. Synthesis of $Na_{3+x} [PV_x W_{12-x} O_{40}]$ , with $x = 1$ to 3, according to Domaille et al. [29]

Compounds  $Na_{3+x} [PV_x W_{12-x} O_{40}]$ , with  $x = 1$  to 3, were synthesised according to modified procedures of Domaille et al. [29], starting from commercially available HPW or the lacunary compound  $Na_{9-x} H_x [PW_9 O_{34}] \cdot x H_2O$ .

$$x = 1$$

Phosphotungstic acid was dissolved in deionised water. The pH value of this solution was 0.5 and was adjusted to 4.8 by addition of small portions of sodium carbonate. In parallel, sodium metavanadate was dissolved in deionised water at 80 °C and added to the previous  $[PW_{11} O_{39}]^{7-}$  solution. The pH value of the combined reaction mixture was adjusted to 2.0, by adding a 2 M hydrochloric acid solution in water, and then heated up to 60 °C. After cooling to room temperature, the pH value was 3.5, and was readjusted to 2.0 using a 2 M hydrochloric acid solution in water. The solution was then reheated to 60 °C. This procedure was repeated once, until upon cooling down to room temperature

the pH value remained stable around 2.0. Finally, the solution was filtered and desalinated by nanofiltration. A yellow solid was obtained.

$$x = 2 \text{ and } 3$$

Sodium acetate was dissolved in deionised water (30 mL), and after dissolution, acetic acid was added, until the pH value of the solution reached 4.8. In the next step, sodium metavanadate and sodium tungstate dihydrate were added, and after dissolution,  $\text{Na}_9\text{xH}_x[\text{PW}_9\text{O}_{34}] \cdot x \text{ H}_2\text{O}$  was added and stirred for 48 h. The colour changed to dark red. It was filtered and the solution was desalinated by nanofiltration. An orange/red solid was obtained.

### 3.6. Synthesis of $\text{Na}_y\text{H}_z[\text{PV}_x\text{W}_{12-x}\text{O}_{40}]$ , with $x = 4$ to 6, via Self-Assembly, Based on the Procedure of Odyakov et al. [20–22]

Sodium metavanadate was dissolved in deionised water, at a temperature of 60 °C. Parallel to this step, sodium tungstate dihydrate was dissolved in deionised water, and an 85% solution of phosphoric acid in water was added. The solution was boiled and the aqueous sodium metavanadate solution was added dropwise. After the addition, the solution turned light brown and the final pH value was 7.5, which was adjusted to 1.5 using a 2 M hydrochloric acid solution in water. The dark brown solution was refluxed for 60 min. After cooling to room temperature, the solution was filtered and desalinated by nanofiltration. An intense red coloured solid was obtained.

### 3.7. Nanofiltration

Nanofiltration for removing the salts was performed using the setup developed by Esser et al. [52].

### 3.8. Etherate Method

The sodium salt  $\text{NaPV}_x\text{W}$ , was dissolved in deionised water, and a hydrochloric acid solution in water was added. In a separation funnel, the acidified solution was mixed with diethyl ether. Upon separation of the phases, a third new, oily, and heavy phase, with an intense colour, was formed at the bottom. The POM ether phase was separated. New acid fractions were added to the aqueous phase and the process was repeated until formation of the third, heavy phase was no longer observed. The combined POM ether phases were dried under reduced pressure, to yield a solid product (Figure S49, Supplementary Materials).

## 4. Conclusions

In summary, we have successfully synthesised a series of vanadium(V)-substituted phosphomolybdates ( $\text{HPV}_x\text{Mo}$ ) and phosphotungstates ( $\text{NaPV}_x\text{W}$ ), with substitution degrees ( $x$ ) of up to 6. All the molybdates are known in the literature, but especially the higher substituted tungstates ( $x > 3$ ) have not been discussed and analysed in the literature yet in such detail. The molybdates were prepared using a self-assembly approach. Tungstates with  $x = 1$  to 3 were synthesised using a lacunary approach, and tungstates with  $x = 4$  to 6 were prepared using a self-assembly route. In order to obtain the respective free acids, acidic, aqueous solutions of the sodium salts of the tungstates were treated with diethyl ether, with the goal of extracting the protonated tungstates. However, this route is progressively limited by low yields and significant losses of the substitution metals, and is therefore not applicable to tungstates with higher V content.

We have comprehensively characterised the V-substituted Keggin POMs and compared the spectroscopic and electrochemical properties of the molybdates and tungstates  $\text{NaPV}_x\text{W}$ , with  $x = 1$  to 6. Comparing the IR and Raman spectra, we found that the vibrational bands of the tungstates are shifted to higher wavenumbers in comparison to the molybdates, due to the higher mass of tungsten. The higher mass difference between W(VI) and V(V), in comparison to Mo(VI) and V(V), leads to the property that different P–O vibrational bands are observed in the IR spectra for the tungstates.

From the NMR spectroscopic investigations, we concluded that both the  $^{31}\text{P}$  and  $^{51}\text{V}$  signals of the tungstates are observed at significantly lower chemical shifts than the signals of the molybdates. We attribute this effect to the increased shielding effect of tungsten, caused by its higher electron density. With increasing degree of substitution with V(V), the  $^{31}\text{P}$  signals of the tungstates appear at more positive values. This effect is attributed to the deshielding effect of the V(V). For both the molybdates and the tungstates, significantly more signals are observed with increasing degree of substitution, as more positional isomers are possible.

By applying UV-Vis spectroscopy, we found the following trend for the LMCT energies:  $\lambda_{\text{Mo(VI)}} < \lambda_{\text{W(VI)}} < \lambda_{\text{V(V)}}$ . For the extinction coefficients, the trend seems to be  $\varepsilon_{\lambda}^{\text{V(V)}} < \varepsilon_{\lambda}^{\text{W(VI)}} < \varepsilon_{\lambda}^{\text{Mo(VI)}}$ . The higher the degree of substitution, the more significant is the intensity decrease in the Mo(VI)/W(VI) LMCT bands and the more intense becomes the V(V) LMCT band. This trend can also be seen as an indicator for successful substitution.

Finally, the electrochemical properties of the POMs were determined, using CV and SWV measurements. Significantly more redox processes were detected for the molybdates than for the corresponding tungstates. Therefore, the tungstates appear to be much less redox active than the molybdates. For the molybdates, there is a shift in the redox peak potentials depending on the degree of substitution. The results show that, the redox potentials of the POMs can be tuned by changing the framework metal and degree of substitution with an additional foreign element, such as V(V).

Together, the trends from the analytical data show that for subsequent applications of the POMs (e.g., in homogeneous catalysis) substituted molybdates should be used rather than tungstates, since molybdates, in contrast to tungstates, have a richer redox chemistry. In addition, the synthetic route for the molybdates allows the POMs to be isolated as heteropolyacids, providing bifunctionality (both redox and Brønsted acid sites) for catalytic applications. Generating tungstates as free acids is only possible to a very limited extent using our presented extraction method.

We were able to show, using our NMR spectra, that the POM stability decreases with an increasing degree of substitution, which is expressed by the observation of various dissociation peaks. This circumstance can be attributed to the increased anionic charge density of the POMs. However, all our POMs proved to be sufficiently stable during our investigations. Therefore, in the search for specific applications, both in catalysis and in biomedicine, higher substituted POM representatives can be used without limitations.

Overall, this report on the synthesis and spectroscopic, as well as electrochemical, properties, provides a solid foundation for further research on the application of V-substituted phosphomolybdates and -tungstates in catalysis or the biomedical field.

**Supplementary Materials:** The following supporting information can be downloaded at: <https://www.mdpi.com/article/10.3390/inorganics11040138/s1>, UV-Vis, NMR, Infrared and Raman Spectra of all compounds, as well as experimental and crystallographic details. References [53–60] are cited in the supplementary materials.

**Author Contributions:** J.-C.R.: investigation, writing (initial draft), visualisation; J.A.C.: investigation; J.A.: funding acquisition, resources, writing (review and editing); M.J.P.: conceptualisation, project administration, supervision, writing (review and editing). All authors have read and agreed to the published version of the manuscript.

**Funding:** We thank the Hansestadt Hamburg for financially supporting José Aceituno Cruz with the Degree Completion Grant for International Students provided through the University of Hamburg. This research received no further external funding; the APC has been waived by MDPI.

**Data Availability Statement:** Data is provided in the Supplementary Materials, Crystallographic information files (.cif) are available through the joint Cambridge Crystallographic Data Centre and Fachinformationszentrum Karlsruhe Access Structures service under the deposition numbers 2240685 ( $\text{NaPV}_2\text{W}$ ) and 2240686 ( $\text{NaPV}_5\text{W}$ ).

**Acknowledgments:** The authors gratefully thank the Fraunhofer-Zentrum für Angewandte Nanotechnologie CAN for performing thermogravimetric analysis, and the research group of Peter Burger, especially Thomas Marx, for the opportunity to measure CV and SWV. We also thank the elemental analysis service department led by Dirk Eifler for analysing our numerous POM samples.

**Conflicts of Interest:** The authors declare no conflict of interest.

## References

- Reichert, J.; Brunner, B.; Jess, A.; Wasserscheid, P.; Albert, J. Biomass oxidation to formic acid in aqueous media using polyoxometalate catalysts—Boosting FA selectivity by in-situ extraction. *Energy Environ. Sci.* **2015**, *8*, 2985–2990. [[CrossRef](#)]
- Maerten, S.; Kumpidet, C.; Voß, D.; Bukowski, A.; Wasserscheid, P.; Albert, J. Glucose oxidation to formic acid and methyl formate in perfect selectivity. *Green Chem.* **2020**, *22*, 4311–4320. [[CrossRef](#)]
- Albert, J.; Wasserscheid, P. Expanding the scope of biogenic substrates for the selective production of formic acid from water-insoluble and wet waste biomass. *Green Chem.* **2015**, *17*, 5164–5171. [[CrossRef](#)]
- Veith, H.; Voges, M.; Held, C.; Albert, J. Measuring and Predicting the Extraction Behavior of Biogenic Formic Acid in Biphasic Aqueous/Organic Reaction Mixtures. *ACS Omega* **2017**, *2*, 8982–8989. [[CrossRef](#)]
- Albert, J.; Lüders, D.; Bösmann, A.; Guldin, D.M.; Wasserscheid, P. Spectroscopic and electrochemical characterization of heteropoly acids for their optimized application in selective biomass oxidation to formic acid. *Green Chem.* **2014**, *16*, 226–237. [[CrossRef](#)]
- Claußnitzer, J.; Bertleff, B.; Korth, W.; Albert, J.; Wasserscheid, P.; Jess, A. Kinetics of Triphase Extractive Oxidative Desulfurization of Benzothiophene with Molecular Oxygen Catalyzed by HPA-5. *Chem. Eng. Technol.* **2020**, *43*, 465–475. [[CrossRef](#)]
- Bertleff, B.; Claußnitzer, J.; Korth, W.; Wasserscheid, P.; Jess, A.; Albert, J. Catalyst Activation and Influence of the Oil Matrix on Extractive Oxidative Desulfurization Using Aqueous Polyoxometalate Solutions and Molecular Oxygen. *Energy Fuels* **2018**, *32*, 8683–8688. [[CrossRef](#)]
- Bertleff, B.; Goebel, R.; Claußnitzer, J.; Korth, W.; Skiborowski, M.; Wasserscheid, P.; Jess, A.; Albert, J. Investigations on Catalyst Stability and Product Isolation in the Extractive Oxidative Desulfurization of Fuels Using Polyoxometalates and Molecular Oxygen. *ChemCatChem* **2018**, *10*, 4602–4609. [[CrossRef](#)]
- Bertleff, B.; Claußnitzer, J.; Korth, W.; Wasserscheid, P.; Jess, A.; Albert, J. Extraction Coupled Oxidative Desulfurization of Fuels to Sulfate and Water-Soluble Sulfur Compounds Using Polyoxometalate Catalysts and Molecular Oxygen. *ACS Sustain. Chem. Eng.* **2017**, *5*, 4110–4118. [[CrossRef](#)]
- Gumerova, N.I.; Al-Sayed, E.; Krivosudský, L.; Čipčić-Paljetak, H.; Verbanac, D.; Rompel, A. Antibacterial activity of polyoxometalates against Moraxella catarrhalis. *Front. Chem.* **2018**, *6*, 336. [[CrossRef](#)]
- Bijelic, A.; Aureliano, M.; Rompel, A. The antibacterial activity of polyoxometalates: Structures, antibiotic effects and future perspectives. *Chem. Commun.* **2018**, *54*, 1153–1169. [[CrossRef](#)]
- Čolović, M.B.; Lacković, M.; Lalačović, J.; Mougharbel, A.S.; Kortz, U.; Krstić, D.Z. Polyoxometalates in Biomedicine: Update and Overview. *Curr. Med. Chem.* **2019**, *27*, 362–379. [[CrossRef](#)]
- Shigeta, S.; Mori, S.; Kodama, E.; Kodama, J.; Takahashi, K.; Yamase, T. Broad spectrum anti-RNA virus activities of titanium and vanadium substituted polyoxotungstates. *Antiviral Res.* **2003**, *58*, 265–271. [[CrossRef](#)]
- Yamase, T. Anti-tumor, -viral, and -bacterial activities of polyoxometalates for realizing an inorganic drug. *J. Mater. Chem.* **2005**, *15*, 4773. [[CrossRef](#)]
- Tajima, Y.; Nagasawa, Z.; Tadano, J. A Factor Found in Aged Tungstate Solution Enhanced the Antibacterial Effect of  $\beta$ -Lactams on Methicillin-Resistant *Staphylococcus aureus*. *Microbiol. Immunol.* **1993**, *37*, 695–703. [[CrossRef](#)] [[PubMed](#)]
- Shigeta, S.; Mori, S.; Yamase, T.; Yamamoto, N.; Yamamoto, N. Anti-RNA virus activity of polyoxometalates. *Biomed. Pharmacother.* **2006**, *60*, 211–219. [[CrossRef](#)] [[PubMed](#)]
- Chen, L.; San, K.A.; Turo, M.J.; Gembicky, M.; Fereidouni, S.; Kalaj, M.; Schimpf, A.M. Tunable Metal Oxide Frameworks via Coordination Assembly of Preyssler-Type Molecular Clusters. *J. Am. Chem. Soc.* **2019**, *141*, 20261–20268. [[CrossRef](#)] [[PubMed](#)]
- Chen, L.; Turo, M.J.; Gembicky, M.; Reinicke, R.A.; Schimpf, A.M. Cation-Controlled Assembly of Polyoxotungstate-Based Coordination Networks. *Angew. Chem. Int. Ed.* **2020**, *59*, 16609–16615. [[CrossRef](#)]
- Long, D.-L.; Burkholder, E.; Cronin, L. Polyoxometalate clusters, nanostructures and materials: From self assembly to designer materials and devices. *Chem. Soc. Rev.* **2007**, *36*, 105–121. [[CrossRef](#)]
- Odyakov, V.F.; Zhizhina, E.G.; Maksimovskaya, R.I. Synthesis of molybdovanadophosphoric heteropoly acid solutions having modified composition. *Appl. Catal. A Gen.* **2008**, *342*, 126–130. [[CrossRef](#)]
- Odyakov, V.F.; Zhizhina, E.G. New process for preparing aqueous solutions of Mo-V-phosphoric heteropoly acids. *Russ. J. Inorg. Chem.* **2009**, *54*, 361–367. [[CrossRef](#)]
- Odyakov, V.F.; Zhizhina, E.G. A novel method of the synthesis of molybdovanadophosphoric heteropoly acid solutions. *React. Kinet. Catal. Lett.* **2008**, *95*, 21–28. [[CrossRef](#)]
- Raabe, J.-C.; Albert, J.; Poller, M.J. Spectroscopic, Crystallographic, and Electrochemical Study of Different Manganese(II)-Substituted Keggin-Type Phosphomolybdates. *Chem.-A Eur. J.* **2022**, *28*, e202201084. [[CrossRef](#)]

24. Abbessi, M.; Contant, R.; Thouvenot, R.; Hervé, G. Dawson Type Heteropolyanions. 1. Multinuclear ( $^{31}\text{P}$ ,  $^{51}\text{V}$ ,  $^{183}\text{W}$ ) NMR Structural Investigations of Octadeca(molybdotungstovanado)diphosphates  $\alpha$ -1,2,3-[ $\text{P}_2\text{MM}'_2\text{W}_{15}\text{O}_{62}$ ] $n^-$  ( $\text{M}, \text{M}' = \text{Mo}, \text{V}, \text{W}$ ): Syntheses of New Related Compounds. *Inorg. Chem.* **1991**, *30*, 1695–1702. [[CrossRef](#)]
25. Patel, A.; Narkhede, N.; Singh, S.; Pathan, S. Keggin-type lacunary and transition metal substituted polyoxometalates as heterogeneous catalysts: A recent progress. *Catal. Rev.* **2016**, *58*, 337–370. [[CrossRef](#)]
26. Himeno, S.; Takamoto, M.; Ueda, T. Synthesis, characterisation and voltammetric study of a  $\beta$ -Keggin-type  $[\text{PW}_{12}\text{O}_{40}]^{3-}$  complex. *J. Electroanal. Chem.* **1999**, *465*, 129–135. [[CrossRef](#)]
27. Knoth, W.H.; Domaille, P.J.; Farlee, R.D. Anions of the type  $(\text{RMOH}_2)_3\text{W}_{18}\text{P}_2\text{O}_{68}^{9-}$  and  $[\text{H}_2\text{OCO}]_3\text{W}_{18}\text{P}_2\text{O}_{68}^{12-}$ . A reinvestigation of “B.<sub>beta</sub>- $\text{W}_9\text{PO}_{34}^{9-}$ ”. *Organometallics* **1985**, *4*, 62–68. [[CrossRef](#)]
28. Massart, R.; Contant, R.; Fruchart, J.M.; Ciabriani, J.P.; Fournier, M. Phosphorus-31 NMR studies on molybdic and tungstic heteropolyanions. Correlation between structure and chemical shift. *Inorg. Chem.* **1977**, *16*, 2916–2921. [[CrossRef](#)]
29. Domaille, P.J.; Watunya, G. Synthesis and tungsten-183 NMR characterization of vanadium-substituted polyoxometalates based on B-type tungstophosphate  $\text{PW}_9\text{O}_{34}^{9-}$ -precursors. *Inorg. Chem.* **1986**, *25*, 1239–1242. [[CrossRef](#)]
30. Ginsberg, A.P. (Ed.) Vanadium (V) substituted dodecatungstophosphates. In *Inorganic Synthesis*; John Wiley & Sons, Ltd.: Hoboken, NJ, USA, 1990; Volume 27.
31. Tsigdinos, G.A.; Hallada, C.J. Molybdovanadophosphoric Acids and Their Salts. I. Investigation of Methods of Preparation and Characterization. *Inorg. Chem.* **1968**, *7*, 437–441. [[CrossRef](#)]
32. Bridgeman, A.J. Computational Study of the Vibrational Spectra of  $\alpha$ - and  $\beta$ -Keggin Polyoxometalates. *Chem.-A Eur. J.* **2004**, *10*, 2935–2941. [[CrossRef](#)] [[PubMed](#)]
33. Lee, J.K.; Melsheimer, J.; Berndt, S.; Mestl, G.; Schlägl, R.; Köhler, K. Transient responses of the local electronic and geometric structures of vanado-molybdo-phosphate catalysts  $\text{H}_{3+n}\text{PV}_n\text{Mo}_{12-n}\text{O}_{40}$  in selective oxidation. *Appl. Catal. A Gen.* **2001**, *214*, 125–148. [[CrossRef](#)]
34. Xu, M.X.; Lin, S.; Xu, L.-M.; Zhen, S.-L. Crystal structure and properties of  $\text{H}_3[\text{PMo}_{12}\text{O}_{40}] \cdot 3 \text{C}_2\text{H}_6\text{O}$ . *Transit. Met. Chem.* **2004**, *29*, 332–335. [[CrossRef](#)]
35. Poller, M.J.; Bönisch, S.; Bertleff, B.; Raabe, J.; Görling, A.; Albert, J. Elucidating activating and deactivating effects of carboxylic acids on polyoxometalate-catalysed three-phase liquid-liquid-gas reactions. *Chem. Eng. Sci.* **2022**, *264*, 118143. [[CrossRef](#)]
36. Pope, M.T.; Scully, T.F. Geometrical Isomerism Arising from Partial Substitution of Metal Atoms in Isopoly and Heteropoly Complexes. Possibilities for the Keggin Structure. *Inorg. Chem.* **1975**, *14*, 953–954. [[CrossRef](#)]
37. Pettersson, L.; Andersson, I.; Grate, J.H.; Selling, A. Multicomponent Polyanions. 46. Characterization of the Isomeric Keggin Decamolybdovanadophosphate Ions In Aqueous Solution by  $^{31}\text{P}$  and  $^{51}\text{V}$  NMR. *Inorg. Chem.* **1994**, *33*, 982–993. [[CrossRef](#)]
38. Selling, A.; Andersson, I.; Grate, J.H.; Pettersson, L. A Potentiometric and ( $^{31}\text{P}$ ,  $^{51}\text{V}$ ) NMR Study of the Aqueous Molybdo-vanadophosphate System. *Eur. J. Inorg. Chem.* **2000**, *2000*, 1509–1521. [[CrossRef](#)]
39. Weinstock, I.A.; Cowan, J.J.; Barbuza, E.M.G.; Zeng, H.; Hill, C.L. Equilibria between  $\alpha$  and  $\beta$  Isomers of Keggin Heteropolytungstates. *J. Am. Chem. Soc.* **1999**, *121*, 4608–4617. [[CrossRef](#)]
40. Sundaram, K.M.; Neiwert, W.A.; Hill, C.L.; Weinstock, I.A. Relative Energies of  $\alpha$  and  $\beta$  Isomers of Keggin Dodecatungstogallate. *Inorg. Chem.* **2006**, *45*, 958–960. [[CrossRef](#)]
41. Neiwert, W.A.; Cowan, J.J.; Hardcastle, K.I.; Hill, C.L.; Weinstock, I.A. Stability and Structure in  $\alpha$ - and  $\beta$ -Keggin Heteropolytungstates,  $[\text{X}^{n+}\text{W}_{12}\text{O}_{40}]^{(8-n)-}$ , X = p-Block Cation. *Inorg. Chem.* **2002**, *41*, 6950–6952. [[CrossRef](#)]
42. Himeno, S.; Takamoto, M.; Ueda, T. Formation of  $\alpha$ - and  $\beta$ -Keggin-Type  $[\text{PW}_{12}\text{O}_{40}]^{3-}$  Complexes in Aqueous Media. *Bull. Chem. Soc. Jpn.* **2005**, *78*, 1463–1468. [[CrossRef](#)]
43. Evtuguin, D.V.; Neto, C.P.; Rocha, J.; de Jesus, J.D.P. Oxidative delignification in the presence of molybdovanadophosphate heteropolyanions: Mechanism and kinetic studies. *Appl. Catal. A Gen.* **1998**, *167*, 123–139. [[CrossRef](#)]
44. Barreau, K.P.; Lyons, J.E.; Song, I.K.; Barreau, M.A. UV-visible spectroscopy as a probe of heteropolyacid redox properties: Application to liquid phase oxidations. *Top. Catal.* **2006**, *41*, 55–62. [[CrossRef](#)]
45. Song, I.K.; Kim, H.S.; Chun, M.S. On the reduction potential of cation-exchanged heteropolyacids (HPAs). *Korean J. Chem. Eng.* **2003**, *20*, 844–849. [[CrossRef](#)]
46. Yamase, T. Photo- and electrochromism of polyoxometalates and related materials. *Chem. Rev.* **1998**, *98*, 307–325. [[CrossRef](#)]
47. Salavati, H.; Rasouli, N. Synthesis and characterization of supported heteropolymolybdate nanoparticles between silicate layers of Bentonite with enhanced catalytic activity for epoxidation of alkenes. *Mater. Res. Bull.* **2011**, *46*, 1853–1859. [[CrossRef](#)]
48. Raj, N.K.K.; Ramaswamy, A.V.; Manikandan, P. Oxidation of norbornene over vanadium-substituted phosphomolybdc acid catalysts and spectroscopic investigations. *J. Mol. Catal. A Chem.* **2005**, *227*, 37–45. [[CrossRef](#)]
49. Sadakane, M.; Steckhan, E. Electrochemical Properties of Polyoxometalates as Electrocatalysts. *Chem. Rev.* **1998**, *98*, 219–238. [[CrossRef](#)]
50. Hwang, D.Y.; Ha, Y.S.; Kim, S. Electrode-Assisted Wacker Process: Phosphomolybdate-Mediated Oxidation of 1-Butene to Methyl Ethyl Ketone. *Bull. Korean Chem. Soc.* **2001**, *22*, 441–442.
51. Ueda, T. Electrochemistry of Polyoxometalates: From Fundamental Aspects to Applications. *ChemElectroChem* **2018**, *5*, 823–838. [[CrossRef](#)]

52. Esser, T.; Huber, M.; Voß, D.; Albert, J. Development of an efficient downstream process for product separation and catalyst recycling of a homogeneous polyoxometalate catalyst by means of nanofiltration membranes and design of experiments. *Chem. Eng. Res. Des.* **2022**, *185*, 37–50. [[CrossRef](#)]
53. Dolomanov, O.V.; Bourhis, L.J.; Gildea, R.J.; Howard, J.A.; Puschmann, H. OLEX2: A complete structure solution, refinement and analysis program. *J. Appl. Crystallogr.* **2009**, *42*, 339–341. [[CrossRef](#)]
54. SHELX. Available online: <https://www.noah-itn.eu/wp-content/uploads/2019/03/shelx-manual.pdf> (accessed on 22 February 2023).
55. Sheldrick, G.M. A short history of SHELX. *Acta Crystallogr. Sec. A: Found. Crystallogr.* **2008**, *64*, 112–122. [[CrossRef](#)]
56. User Guide to Crystal Structure Refinement with SHELXL. 2008.
57. Hübschle, C.B.; Sheldrick, G.M.; Dittrich, B. ShelXle: A Qt graphical user interface for SHELXL. *J. Appl. Crystallogr.* **2011**, *44*, 1281–1284. [[CrossRef](#)] [[PubMed](#)]
58. Available online: <https://digital-library.theiet.org/content/journals/10.1049/esn.1987.0025?fmt=text> (accessed on 22 February 2023).
59. Spek, A.L.J. Single-crystal structure validation with the program PLATON. *J. Appl. Crystallogr.* **2003**, *36*, 7–13. [[CrossRef](#)]
60. Spek, A.L. PLATON SQUEEZE: A tool for the calculation of the disordered solvent contribution to the calculated structure factors. *Acta Crystallogr. Sec. C: Struct. Chem.* **2015**, *71*, 9–18. [[CrossRef](#)] [[PubMed](#)]

**Disclaimer/Publisher's Note:** The statements, opinions and data contained in all publications are solely those of the individual author(s) and contributor(s) and not of MDPI and/or the editor(s). MDPI and/or the editor(s) disclaim responsibility for any injury to people or property resulting from any ideas, methods, instructions or products referred to in the content.